J. Mol. Biol. (1994) **236**, 817–830

The 1·8 Å Structure of Carbonmonoxy-β_4 Hemoglobin

Analysis of a Homotetramer with the R Quaternary Structure of Liganded $\alpha_2\beta_2$ Hemoglobin

Gloria E. O. Borgstahl†, Paul H. Rogers and Arthur Arnone‡

Department of Biochemistry, The University of Iowa, Iowa City, IA 52242, U.S.A.

The β-chains isolated from the human hemoglobin $\alpha_2\beta_2$ heterotetramer self-assemble to form a β_4 homotetramer. We report the structure of the carbonmonoxy-β_4 ($CO\beta_4$) tetramer refined at a resolution of 1·8 Å. Compared to the three known quaternary structures of human hemoglobin, the T state, the R state and the R2 state, the quaternary structure of $CO\beta_4$ most closely resembles the R state. While the degree of structural similarity between $CO\beta_4$ and the R state of liganded $\alpha_2\beta_2$ is quite high, differences between the α and β-chain sequences result in interesting alternative packing arrangements at the subunit interfaces of $CO\beta_4$. In particular, Arg40β and Asp99β interact across the $CO\beta_4$ equivalent of the $\alpha1\beta2$ interface to form two symmetry-related salt bridges that have no counterpart in either liganded or deoxyhemoglobin. Because these salt bridges are near a 2-fold symmetry axis, steric constraints prevent their simultaneous formation, and electron density images of Arg40β and Asp99β show equally populated dual conformations for the side-chains of both residues. Relative to the liganded $\alpha_2\beta_2$ tetramer, the Arg40β···Asp99β salt bridges introduce ionic interactions that should strengthen the $CO\beta_4$ tetramer. The $CO\beta_4$ equivalent of the $\alpha1\alpha2$ and $\beta1\beta2$ interfaces strengthens the tetramer relative to the liganded $\alpha_2\beta_2$ tetramer by tethering both ends of the central cavity. (The entrance to the central cavity is altered so that the N termini move closer together and the C termini further apart, forming an anion binding pocket that is absent in liganded $\alpha_2\beta_2$ hemoglobin.) In contrast, analysis of the $CO\beta_4$ counterpart of the $\alpha1\beta1$ interface indicates that this interface is weakened in the $CO\beta_4$ tetramer. These differences in interface stability provide a structural explanation for the published observation that the $\alpha_2\beta_2$ tetramer assembles *via* a stable $\alpha1\beta1$ dimer intermediate, whereas assembly of the $CO\beta_4$ tetramer is characterized more accurately by a monomer-tetramer equilibrium.

Keywords: X-ray crystal structure; hemoglobin; R state; quaternary structure; conformational heterogeneity

1. Introduction

Equimolar amounts of α and β-chains of human hemoglobin (Hb§) self-assemble to form $\alpha_2\beta_2$ heterotetramers. Interestingly, isolated β-chains aggregate to form β_4 homotetramers but isolated α-chains form dimers (Benesch & Benesch, 1974; Valdes & Ackers, 1977). Comparison of the $\alpha_2\beta_2$ and β_4 subunit interfaces at 2·5 Å resolution (Arnone *et al.*, 1982) revealed a very high degree of similarity between the quaternary structures of carbonmonoxy-β_4 ($CO\beta_4$) and carbonmonoxy-Hb (COHb), a structural similarity that is remarkable in view of the 84 sequence differences between human α (141 residue) and β (146 residue) chains, many of which are located at the subunit interfaces.

Unlike the $\alpha_2\beta_2$ tetramer, the β_4 tetramer has high oxygen affinity, does not bind oxygen cooperatively, and is influenced much less by allosteric effectors of native Hb oxygen affinity (Kurtz *et al.*, 1981). Also, the α and β subunits of Hb assemble to form a tetramer *via* a very stable $\alpha\beta$ dimer intermediate, whereas β_4 assembles from monomeric β-chains with relatively little dimer formation (Valdes & Ackers, 1977; Philo *et al.*, 1988). Additionally, while the $\alpha_2\beta_2$ tetramer has much lower oxygen

† Present address: The Scripps Research Institute, La Jolla, CA 92037, U.S.A.

‡ Author to whom all correspondence should be addressed.

§ Abbreviations used: Hb, hemoglobin; oxyHb(R), R state oxy $\alpha_2\beta_2$ Hb; deoxyHb(T), T state deoxy $\alpha_2\beta_2$ Hb; COHb(R2), R2 state carbonmonoxy $\alpha_2\beta_2$ Hb; deoxyβ_4, deoxy β_4 Hb; $CO\beta_4$, carbonmonoxy β_4 Hb; COMb, carbonmonoxy myoglobin; r.m.s., root-mean-square; DPG, diphosphoglycerate.

0022-2836/94/080817-14 $08.00/0

affinity than isolated subunits, the β_4 tetramer exhibits the opposite phenomenon termed quaternary enhancement. That is, the association of monomeric β-chains to β_4 actually results in an increase in oxygen affinity (Valdes & Ackers, 1978).

In this and the accompanying paper (Borgstahl *et al.*, 1993), we report high-resolution structures of carbonmonoxy- and deoxy-β_4, respectively. These structures provide additional insights into the relationships between Hb structure and function.

2. Materials and Methods

(a) *Collection of diffraction data*

$CO\beta_4$ crystals (space group $P2_1$ with $a=63{\cdot}3$ Å, $b=82{\cdot}4$ Å, $c=53{\cdot}7$ Å and $\beta=90{\cdot}1°$) were grown as previously described (Arnone & Briley, 1978) and were mounted in quartz capillaries in a carbon monoxide atmosphere. Diffraction data were collected on 2 crystals with a Rigaku AFC6R diffractometer that was fitted with a San Diego Multiwire Systems area detector. The data were scaled and merged as described by Howard *et al.* (1987). A total of 53,563 unique reflections (423,044 total) were collected, representing 94·7% of the possible data out to a resolution of 1·74 Å. The data are 99·4% complete out to a resolution of 1·81 Å, and 75·9% complete in the 1·81 to 1·74 Å shell. The diffraction data are of high quality as judged by an R_{symm} value of 4·75% on intensity for all data.

(b) *Structure determination and refinement*

The initial structure of $CO\beta_4$ was solved at 2·5 Å resolution by a combination of single derivative isomorphous replacement and molecular replacement (Arnone & Briley, 1978; Arnone *et al.*, 1982). The starting atomic model was further refined against the original 2·5 Å data to an R-value of 17·4% through iterative cycles of manual rebuilding with the program TOM/FRODO (Cambillau, 1989; Jones, 1985) and least-squares refinement with the program TNT (Tronrud *et al.*, 1987). At this point, the 1·74 Å resolution data were collected. Analysis of the 2·5 Å atomic model indicated that one subunit (β4) had slightly irregular heme geometry. To ensure that this anomaly was not due to a modeling error, the β1 subunit was carefully fit to 1·74 Å F_o-F_c omit maps and then placed in the positions of the other 3 subunits by least-squares superposition. The resulting model was fit to F_o-F_c omit maps and refined with TNT to an R-value of 19·0%. This improved the heme stereochemistry significantly. PROLSQ was used in the last stages of refinement to allow for the easy addition of residues with dual conformations (Sheriff, 1987; Sheriff & Hendrickson, 1987). The final R-value was 17·7%.

Water molecules and residues with dual conformations were identified systematically in F_o-F_c electron density maps using the programs PEAKS and ANAL_PEAKS to locate and then classify peaks by their distances from the atomic model (Borgstahl, 1992). Water molecules with peak intensity greater than 3 times the r.m.s. value of the F_o-F_c map were retained if they (1) remained near their original position, (2) retained a hydrogen bond partner, and (3) maintained a temperature factor below 60 Å^2. Overlapping solvent sites were observed, but not modeled (Smith *et al.*, 1988). Dual conformers were identified by (1) peaks that were too close to the atomic model to be accounted for as solvent, (2) peaks not consistent with solvent stereochemistry, and (3) manually modeled low-energy side-chain rotamers that refined to a high-energy conformation. The main-chain was refined with only one conformation and the occupancies of dual conformers were fixed at 0·5. This systematic search of high resolution F_o-F_c maps revealed dual conformers not observed in the earlier work (Arnone *et al.*, 1982).

3. Results and Discussion

(a) *Quality of structure*

The refined atomic model of $CO\beta_4$ at 1·8 Å resolution consists of 4620 non-hydrogen protein atoms, four CO-heme groups, 132 water molecules and four sulfate ions. This structure has very good stereochemistry, with r.m.s. deviations from ideal geometry of 0·015 Å for bond lengths and 0·33 Å for bond angle distances. The average temperature factor is 30·7 Å^2 (29·9 Å^2 for the protein atoms alone). The average water temperature factor is 41·7 Å^2 (standard deviation = 9·6) with a minimum of 20·2 Å^2 and a maximum of 59·2 Å^2.

Dual conformers are becoming a common feature of carefully refined high-resolution structures (Svensson *et al.*, 1986). In particular, dual conformations are included in several globin structures (Phillips, 1980; Smith *et al.*, 1986; Kuriyan *et al.*, 1986; Tilton & Petsko, 1988; Arents & Love, 1989). Also, side-chains with two positions were noted in the high-salt 1·74 Å structure of deoxyHb (Fermi *et al.*, 1984). In the final stages of the refinement of the $CO\beta_4$ atomic model 35 residues were modeled with dual conformations (see Table 1).

Since the asymmetric unit in β_4 crystals is a tetramer, each β subunit was modeled and refined individually. Coordinate differences between the four chemically equivalent β subunits were used as an estimate of error in the atomic model (Table 2). The average r.m.s. deviation in main-chain atomic positions, σ_p, was calculated after least-squares superposition of backbone atoms of individual subunits. The value of σ_p includes structural differences due to crystal lattice contacts as well as random errors and modeling errors, so it may be an overestimate of the error. Therefore, a second parameter, σ_{pc}, was also calculated in which only internal "core" main-chain atoms were superimposed. Since the largest errors in atomic position tend to be associated with surface residues that have higher mobility and weaker electron density, σ_{pc} may be an underestimate of the intrinsic error in the atomic model. The error estimates of $\sigma_p=0{\cdot}37$ Å and $\sigma_{pc}=0{\cdot}17$ Å for $CO\beta_4$ are typical for a high-resolution protein structure.

(b) *Nomenclature*

The correspondence between the subunits of the β_4 homotetramer and those of the $\alpha_2\beta_2$ heterotetramer is such that β1 coincides with α1, β2 with β1, β3 with α2, and β4 with β2. For clarity, our nomenclature includes parenthetical reference to the corresponding heterotetramer interface. For example, $\beta1\beta4(\alpha1\beta2)$ indicates that the homo-

Table 1
$CO\beta_4$ residues with dual conformations

β1		β2		β3		β4	
		Glu6(A3)	S				
				Leu14(A11)	B		
		—		Glu26(B8)	S		
Arg40(C6)	I	Arg40(C6)	I,L	Arg40(C6)	I	Arg40(C6)	I
		Glu43(CD3)	S	Glu43(CD3)	S,L	Glu43(CD3)	S,L
				Leu68(E12)	B	Leu68(E12)	B
Phe71(E15)	B	Phe71(E15)	B	Phe71(E15)	B	Phe71(E15)	B
Leu75(E19)	B	Leu75(E19)	B	—			
		—		Lys82(EF6)	S		
Val98(FG5)	B	Val98(FG5)	B	Val98(FG5)	B	Val98(FG5)	B
Asp99(G1)	I	Asp99(G1)	I	Asp99(G1)	I	Asp99(G1)	I
Cys112(G14)	I	Cys112(G14)	I	Cys112(G14)	I	Cys112(G14)	I
		His117(G19)	S			His117(G19)	S
		Glu12(GH4)	S,L	Glu121(GH4)	S		

The residue environment is indicated by S (surface residue), L (lattice contact), B (buried side-chain), and I (subunit–subunit interface).

tetramer $\beta1\beta4$ interface corresponds to the $\alpha1\beta2$ interface of the heterotetramer. Similarly, the other β_4 interfaces are referred to as $\beta2\beta3(\alpha2\beta1)$, $\beta1\beta3(\alpha1\alpha2)$, $\beta2\beta4(\beta1\beta2)$, $\beta1\beta2(\alpha1\beta1)$ and $\beta3\beta4(\alpha2\beta2)$.

(c) *Crystal lattice contacts and asymmetry*

While it is clear that crystal lattice contacts do not cause energetically large deformations in protein structure, they can produce small localized perturbations that may influence the functional characteristics of a protein in the crystalline state. In the case of the β_4 crystal lattice, each β subunit has a different set of lattice contacts. The values of σ_p listed in Table 2 provide a coarse measure of tetramer asymmetry. Compared to an average σ_p value of 0·37 Å, subunits $\beta1$ and $\beta3$ are the most similar ($\sigma_p = 0{\cdot}25$ Å), while subunits $\beta2$ and $\beta4$ differ the most ($\sigma_p = 0{\cdot}44$ Å). However, the impact of intertetramer lattice contacts can be documented more accurately by correlating the location of lattice contacts with subunit differences in atomic mobility and tertiary structure. This is accomplished in Figure 1 by plotting temperature factor and positional asymmetry *versus* residue number, and by categorizing lattice contacts by type (van der Waals, salt bridges and hydrogen bonds) and by interaction distance. If the residues involved in a lattice interaction also have low mobility (i.e. low temperature factors), the interaction is probably energetically significant. This type of analysis can identify which subunits are least influenced by lattice forces and presumably the most representative of solution behavior.

Table 2
$CO\beta_4$ error estimates

	σ_p†	σ_{pc}‡
$\beta1$ & $\beta2$	0·44	0·19
$\beta1$ & $\beta3$	0·25	0·16
$\beta1$ & $\beta4$	0·35	0·16
$\beta2$ & $\beta3$	0·41	0·20
$\beta2$ & $\beta4$	0·44	0·20
$\beta3$ & $\beta4$	0·32	0·13
Average	0·37	0·17

† The r.m.s. deviation in main-chain atoms after pairwise least-squares superposition of all main-chain atoms of specified subunits.

‡ The internal core residues were defined as areas showing low average main-chain *B* values and little asymmetry in Fig. 1. The segments included in the calculation were B9 to C7 (27 to 41), E3 to E16 (59 to 72), F1 to G16 (85 to 114) and H1 to HC3 (123 to 146) for β subunits.

The presence of lattice contacts (Fig. 1) correlates with lower temperature factors, indicating that residues involved in, or neighboring, intertetramer contacts have decreased mobility. Similarly, the largest peaks correlate well with regions that have multiple close lattice contacts. In particular, crystal lattice interactions perturb the CD corner and D helix of subunit $\beta4$ where residues 43(CD2) through 58(E2) are shifted relative to the other subunits (Fig. 1(c), (e) (f)). These residues are located in the most extensive lattice contact region. $\beta4$ residues CD2, CD3 and CD5 interact with six residues on the A helix of an adjacent $\beta4$ subunit, and $\beta4$ residues D3, D4, D6, D7, E1 and E4 interact with residues A13, A15, B1, B3, B4 and E5 on a neighboring $\beta2$ subunit to form a total of 70 non-covalent interactions. The position of Glu43(CD2) $\beta4$ is clearly influenced by multiple intermolecular hydrogen bonds and salt bridges. Together, the force of these energetically significant lattice contacts shift the position of the $\beta4$ CD corner and D helix by 2 to 13 times σ_{pc}.

Pairwise comparisons of the β subunits indicate that $\beta1$, $\beta2$ and $\beta3$ are perturbed the least by crystal contacts. Compared to $\beta4$, these subunits have half the number of lattice contacts and significantly higher average temperature factors. However, $\beta2$ has a few more lattice contacts than $\beta1$ or $\beta3$, and as shown in Figure 1(a), (d), (f), $\beta2$ residues A13 through B4 are perturbed by a cluster of 39 lattice contacts with $\beta4$ residues D3 through E2. Also, the

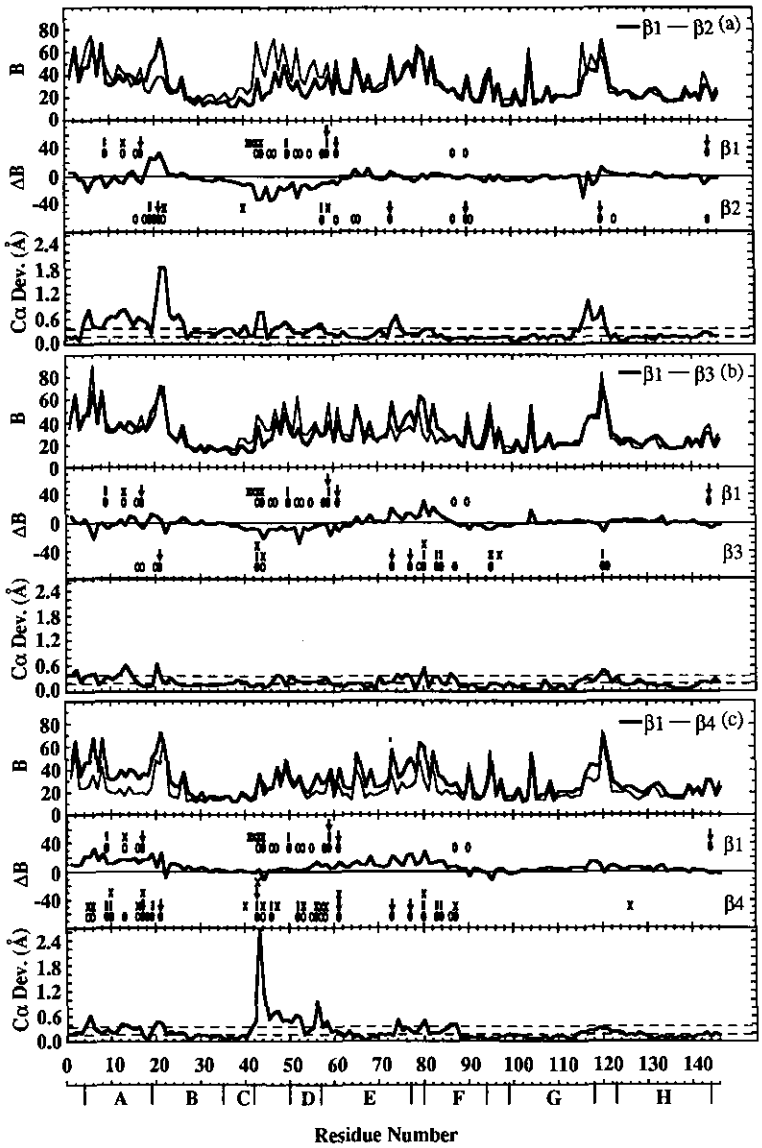

Fig. 1.

heme propionates of $\beta 2$ and $\beta 3$ form an inter-tetramer hydrogen bond and salt bridge, respectively. Nevertheless, $\beta 1$ and $\beta 3$ have almost identical tertiary structures and atomic temperature factors (Fig. 1(b)), and therefore the functional properties of $\beta 1$ and $\beta 3$ (e.g. ligand binding properties) are likely to be affected the least by the crystal environment.

(d) *Heme-CO ligand stereochemistry*

The stereochemistry of the bound CO ligand is compared in Table 3 for $CO\beta_4$, COHb(R) (COHb in the R-state determined at 2·2 Å resolution with crystals grown from high salt solutions (Derewenda *et al.*, 1990)), and COHb(R2) (the R2-state structure of COHb determined at 1·7 Å resolution with crystals grown from relatively low salt solutions (Silva *et al.*, 1992)). The crystals of $CO\beta_4$ were grown under oxygen-free conditions in the presence of a reducing agent in order to avoid oxidation and ensure full CO occupancy. It is not possible to estimate atomic occupancies accurately at this

Table 3

CO ligand stereochemistry in hemoglobin β subunits

	COHb† (R state)	COHb‡ (R2 state)	$CO\beta_4$‡ (R state)	Average
A. *Angles (deg.)*				
Fe–C–O	171	167 (4)	172 (2)	170
Fe–C & heme normal	6	6 (2)	7 (2)	6
B. *Distances (Å)*				
Fe–C	1·77	1·76 (1)	1·78 (1)	1·77
His(E7)$N^{\varepsilon 2}$···O	3·30	3·23 (4)	3·29 (4)	3·27
His(E7)$C^{\delta 2}$···O	3·35	3·34 (2)	3·23 (3)	3·31
Val(E11)$C^{\gamma 1}$···O	3·28	3·19 (1)	3·09 (6)	3·19

† Derewenda *et al.* (1990).

‡ Standard deviations of mean values ×100 are reported in parentheses.

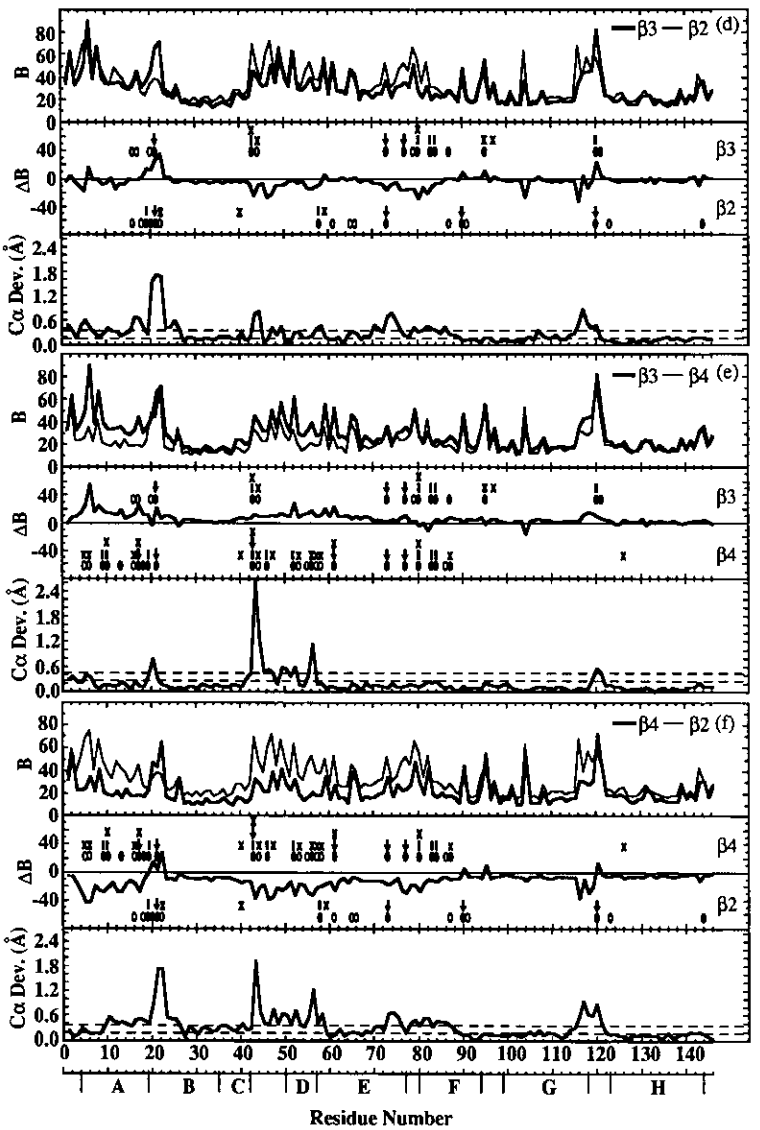

Figure 1. Correlation of temperature factor and positional asymmetry with intertetramer contacts in the $CO\beta_4$ crystal lattice. The temperature factor differences and C^{α} deviations between $CO\beta_4$ subunits are plotted *versus* residue number for (a) $\beta 1$ *versus* $\beta 2$, (b) $\beta 1$ *versus* $\beta 3$, (c) $\beta 1$ *versus* $\beta 4$, (d) $\beta 3$ *versus* $\beta 2$, (e) $\beta 3$ *versus* $\beta 4$, and (f) $\beta 4$ *versus* $\beta 2$. Crystal lattice contacts indicated by ◊ include atom pairs within 4·0 Å, ♦ atom pairs within 3·5 Å, ↓ salt bridges, | hydrogen bonds, × contacts through a water molecule within 4·0 Å, and × contacts through a water molecule within 3·5 Å. C^{α} deviations after least-squares superposition of all main-chain atoms are shown in the bottom third of each panel. Estimates of positional error, σ_p(avg) and σ_{pc}(avg), are indicated by broken horizontal lines. The 8 β-chain helices (designated A through H) are indicated below their corresponding residue numbers.

resolution, but strong electron density and low temperature factors for the CO atoms (average B values of 14·7 Å^2 and 15·7 Å^2 for the C and O atoms, respectively) indicate that full occupancy was achieved. Similarly, the COHb(R2) structure has average atomic temperature factors of 17·7 Å^2 and 18·9 Å^2 for the C and O atoms, respectively.

In carrying out the refinement of $CO\beta_4$ and the R2 state of COHb, the Fe–C and C–O bond lengths were restrained, but the bond angles were not. Unlike carbonmonoxymyoglobin (COMb), where the CO ligand has two conformations (Kuriyan *et al.*, 1986), $CO\beta_4$, COHb(R) and COHb(R2) bind CO in a single well-defined conformation. In particular, the CO ligand is positioned midway between His63(E7) and Val67(E11) with 3·1 Å to 3·3 Å van der Waals contacts between the ligand O atom and His(E7)$N^{\varepsilon 2}$, His(E7)$C^{\delta 2}$, and Val(E11)$C^{\gamma 1}$. For $CO\beta_4$, the next closest contacts for the ligand O atom are 3·8 Å and 3·9 Å to Leu28(B10)$C^{\delta 1}$ and Phe42(CD1)C^{ζ}. Derewenda *et al.* (1990) reported that the CO ligands of COHb(R) are bent by ~10° from linearity with the heme Fe and the heme normal. This is in contrast to simple unhindered CO-porphyrins, where the Fe–C–O group is linear and aligns with the heme normal (Peng & Ibers, 1976), or to COMb, where the two Fe–C–O conformations have bond angles of 120° and 141°. Derewenda *et al.* (1990) noted that in COHb(R) "the amount of bending that emerged from the refine-

ment was barely significant, but is corroborated by the electron density", and that the bend is away from distal residues His(E7) and Val(E11). The COHb(R2) and $CO\beta_4$ structures confirm the magnitude and direction of the CO ligand bending, and indicate that it is due to interactions with His(E7) and Val(E11).

(e) *Quaternary structure characterization*

(i) *Iron-iron distances*

At 4·4 Å resolution, Arnone & Briley (1978) observed that the iron-iron distances of $CO\beta_4$ were closer to metHb than to deoxyHb. We now can compare the quaternary structure of $CO\beta_4$ with three different quaternary structures for human Hb: deoxyHb(T) (the T-state structure of human deoxyHb determined from crystals grown in high-salt solutions and refined first at 1·7 Å (Fermi *et al.*, 1984) and then at 1·5 Å resolution (Kavanaugh *et al.*, 1992)), oxyHb(R), and COHb(R2). Clearly, the $CO\beta_4$ iron distances in Figure 2 are very similar to those of the liganded Hb structures and quite different from those of deoxyHb(T). However, while the $CO\beta_4$ iron distances are somewhat closer to oxyHb(R) than COHb(R2), the differences are small and difficult to interpret. These distances are only a rough measure of quaternary structure and a comparison of the subunit-subunit interfaces is a much more accurate measure of quaternary structure similarities.

(ii) *Comparison of the $CO\beta_4$ quaternary structure with the R and R2 states of liganded hemoglobin*

To compare quaternary structures, the main-chain atoms of one subunit of $CO\beta_4$ were superimposed on the corresponding atoms of a β subunit of the oxyHb(R) or COHb(R2) tetramers (Figs 3 and 4). The β subunits of both the oxyHb(R) and COHb(R2) tetramers superimpose very well with $CO\beta_4$. That is, there is relatively little difference in the tertiary structure (see the bottom superimposed subunits in Fig. 3(a) and (b)). On the other hand, the non-superimposed β/α pairs show significant differences in quaternary structure between $CO\beta_4$ and both oxyHb(R) and COHb(R2). The C^α deviations range from ~1 Å to ~10 Å for the $CO\beta_4$/oxyHb(R) β/α pairs and from ~2 Å to ~15 Å for the $CO\beta_4$/COHb(R2) β/α pairs, indicating that the quaternary structure of $CO\beta_4$ is closer to oxyHb(R).

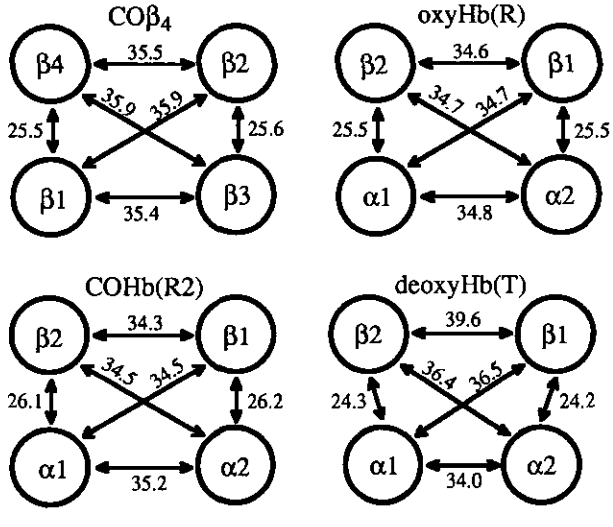

Figure 2. Comparison of the heme iron-iron distances (Å) of $CO\beta_4$ with oxyHb(R), COHb(R2) and deoxyHb(T). The correspondence between the β_4 homotetramer subunits and the $\alpha_2\beta_2$ heterotetramer subunits is as described in Results and Discussion, section (b).

The nature of the quaternary structure differences associated with the $\beta1\beta4(\alpha1\beta2)$ interface is illustrated in Figure 3(a) and (b). The $CO\beta_4$ quaternary structure differs from the R state by a rotation of 8·1° about the joint region (Fig. 3(a)). Transition from the R state to the R2 state involves a subsequent rotation of 12·2° about the joint region (not shown). That is, these quaternary structures can be organized in the order $CO\beta_4$-R-R2 by ordered rotations of 8·1° and 12·2° about very similar axes that pass through the joint region (Fig. 3(b)). Thus, the quaternary structure of $CO\beta_4$ is necessarily much closer to that of the R state than the R2 state. While these transitions have very little affect on the joint region, the switch region changes from a tightly packed structure in $CO\beta_4$ to a very open structure in the R2 state.

The two other $CO\beta_4$ subunit interfaces are compared to the analogous oxyHb(R) interfaces in Figure 4. The $\beta2\beta4(\beta1\beta2)$ interfaces of $CO\beta_4$ and oxyHb(R) differ mainly by a simple translation of about 4 Å. This translation alters the entrance to the central cavity in the $CO\beta_4$ tetramer by increasing the distance between the C-terminal peptides and decreasing the distance between the *N*-terminal peptides (see Fig. 4(a)). This change creates two symmetry-related sulfate binding sites that are separated by 6·5 Å, exactly the distance between the phosphate groups of an extended molecule of DPG providing a structural explanation for the observation reported by Benesch *et al.* (1968) that oxyβ_4 has a much higher affinity for DPG than oxyHb.

The $\alpha1\beta1$ (and symmetry-related $\alpha2\beta2$) interface displays pseudo 2-fold symmetry and is constructed from the ends of the B and G helices, the beginning of the H helices, and the GH corners of the α and β-chains. This is a static interface that undergoes very little structural change between liganded and deoxyHb. Figure 4(b) reveals that the structural differences between $CO\beta_4$ and oxyHb(R) at the $\beta3\beta4(\alpha2\beta2)$ interface are not as large as those at the other interfaces. The C^α deviations of the non-superimposed α/β pairs are about 1 Å at the B helix, while the end of the G helix and the beginning of the H helix aligned to within 0·5 Å. Nevertheless, the intersubunit contacts between the $\beta3(\alpha2)$ B helix and the $\beta4(\beta2)$ H helix are increased slightly in $CO\beta_4$, indicating that the oxyHb(R) $\alpha2\beta2$ interface is more closely packed in this region. The difference

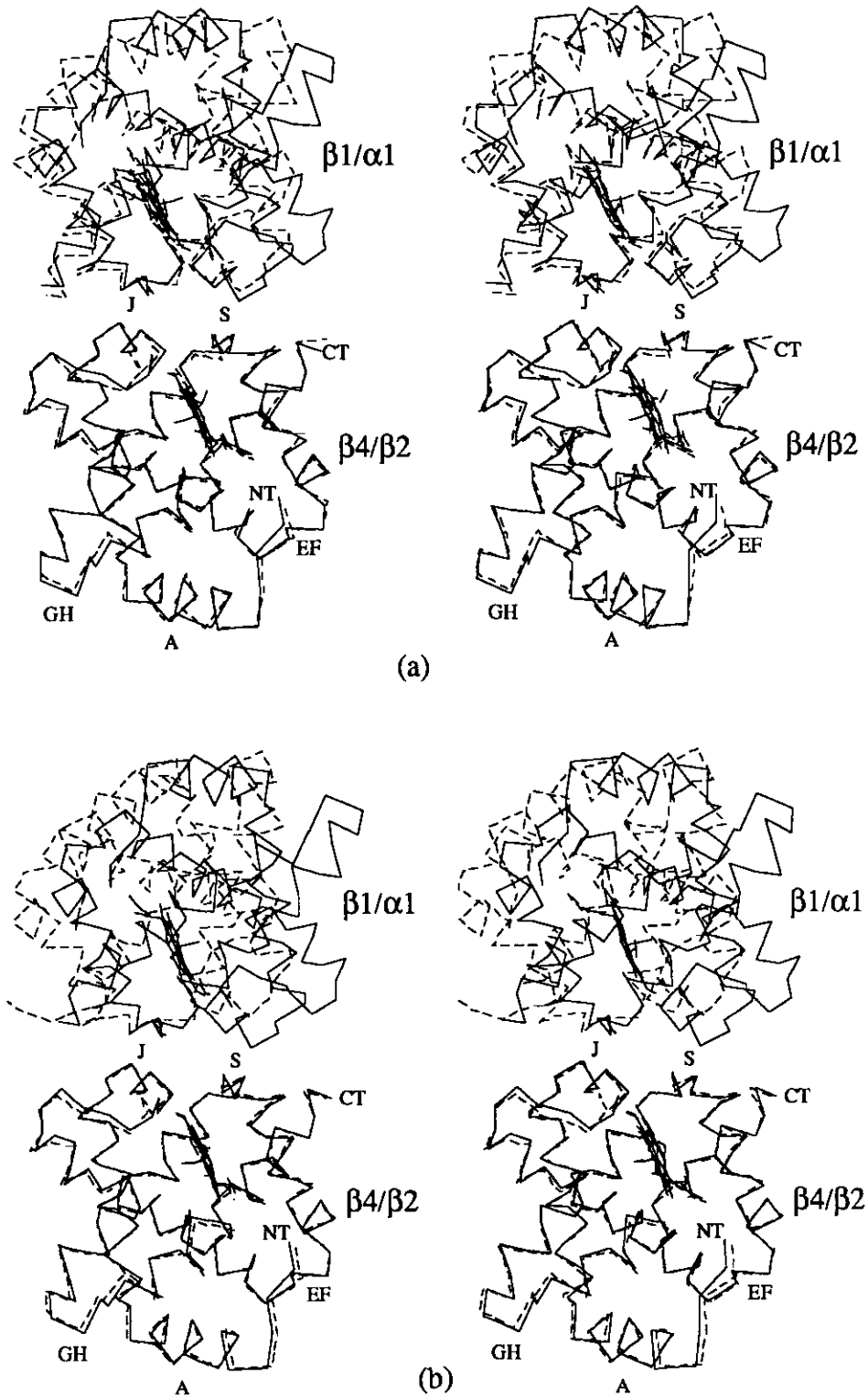

Figure 3. Stereo C^{α} tracings showing the differences in quaternary structure between the $\alpha 1\beta 2$ dimer of oxyHb(R) or COHb(R2) and the corresponding $\beta 1\beta 4$ dimer of $CO\beta_4$. In (a) oxyHb(R) is drawn with broken lines, $CO\beta_4$ with continuous lines. In (b) COHb(R2) is drawn with broken lines, $CO\beta_4$ with continuous lines. The main-chain atoms of the β_4 subunit of $CO\beta_4$ and the $\beta 2$ subunit of oxyHb(R) or COHb(R2) were superimposed (only residues 14 to 20, 23 to 40, 48 to 74, 77 to 93, 96 to 116 and 122 to 143 were included in the calculation) with r.m.s. deviations of 0·37 Å and 0·34 Å, respectively. The switch region (S), the joint region (J), selected helices, and the N and C termini are labeled.

at the GH corner is due primarily to the amino acid substitutions Gly119(GH2)$\beta \rightarrow$Pro114(GH2)α and Lys120(GH3)$\beta \rightarrow$Ala115(GH3)α.

Thus, despite the many amino acid differences between β and α subunits, the β_4 homotetramer is assembled in a manner that is remarkably similar to

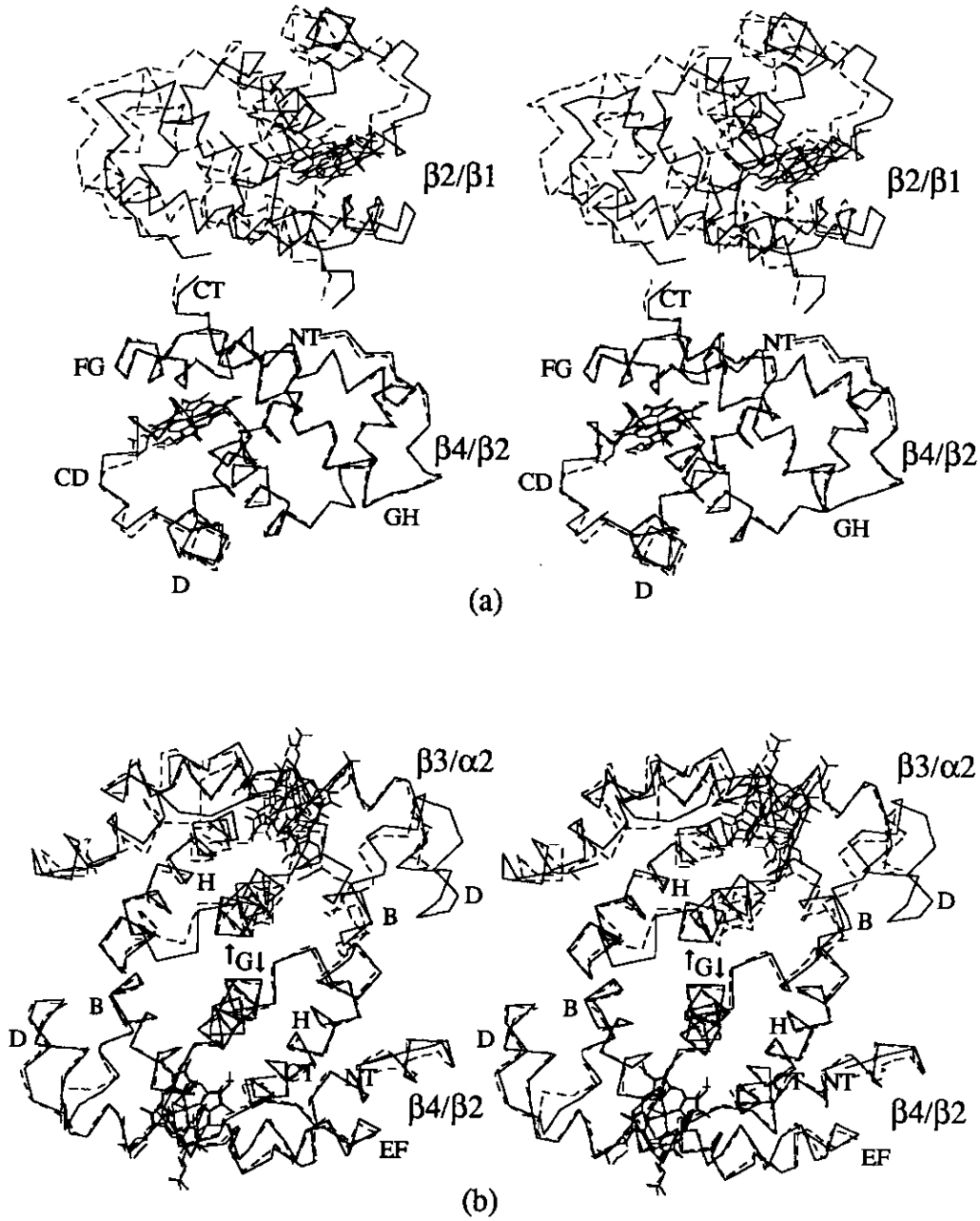

Figure 4. Stereo C^{α} tracings showing the differences in quaternary structure between the $\beta 1\beta 2$ (a) or $\alpha 2\beta 2$ (b) dimers of oxyHb(R) and the corresponding $\beta 2\beta 4$ and $\beta 3\beta 4$ dimers of $CO\beta_4$. OxyHb(R) is drawn with dashed lines, $CO\beta_4$ with continuous lines.

the $\alpha_2\beta_2$ heterotetramer. Compared to the two known liganded $\alpha_2\beta_2$ quaternary structures (R and R2), $CO\beta_4$ most closely resembles the R quaternary structure. However, there are significant structural differences between $CO\beta_4$ and the R state of liganded Hb at all the subunit-subunit interfaces; differences that are the basis for the unique functional properties of the β_4 tetramer.

(iii) *Interface residues with dual conformations*

In the $CO\beta_4$ tetramer residues Arg40(C6) and Asp99(G1) form two symmetry-related salt bridges across the $\beta 1\beta 4(\alpha 1\beta 2)$ interface (Fig. 5), salt bridges that do not have counterparts in the $\alpha 1\beta 2$ interface of either deoxy or liganded $\alpha_2\beta_2$ Hb. It is also possible for Arg40 and Asp99 to form intrasubunit interactions, but the *syn* stereochemistry of these salt bridges is less favorable than the *anti* stereochemistry of the intersubunit salt bridges (Ippolito *et al.*, 1990). Because both the inter- and intrasubunit salt bridges form near the dyad axis between the $\beta 1$ and $\beta 4$ subunits, steric conflicts prevent their simultaneous formation (Fig. 5), and electron density images of Arg40β and Asp99β show equally populated dual conformations for the sidechains of both residues (Fig. 6(a) and (b)). That is, only one of four possible Arg40···Asp99 salt bridges

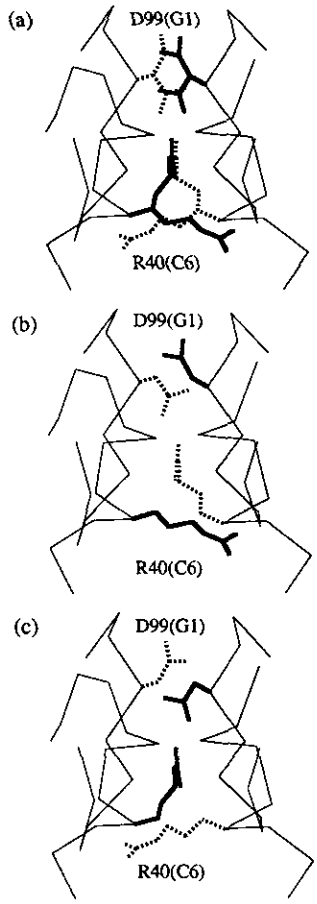

Figure 5. The Arg40(C6)···Asp99(G1) salt bridge at the $\beta1\beta4(\alpha1\beta2)$ interface of $CO\beta_4$. In (a) the dual conformations of Arg40(C6) and Asp99(G1) are overlaid. The 2 equivalent intersubunit salt bridges are shown in (b) and (c). The dual conformations of Arg40 and Asp99 are the result of steric conflicts that prevent both salt bridges from forming simultaneously.

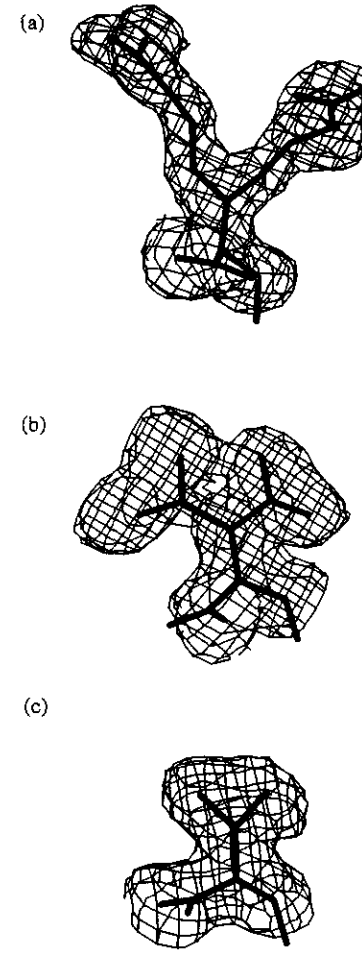

Figure 6. F_o-F_c omit electron density maps (contoured at 2σ) showing the dual conformations of (a) Arg40(C6)$\beta4$, (b) Asp99(G1)$\beta1$ both at the $\beta1\beta4(\alpha1\beta2)$ interface and (c) Cys112(G14)$\beta4$ at the $\beta3\beta4(\alpha2\beta2)$ interface. Drawing made using XtalView (McRee, 1992).

can exist at a time in a given $\beta1\beta4$ (or $\beta2\beta3$) dimer, and the 222 symmetry of the $CO\beta_4$ tetramer is violated.

Another dyad-generated steric conflict results in dual conformations for Cys112(G14) at the $\beta1\beta2(\alpha1\beta1)$ interface. The amino acid difference Val107(G14)α→Cys112(G14)β at the $\beta1\beta2(\alpha1\beta1)$ interface creates a packing defect and Cys112β compensates by adopting two conformations. In fact, the electron density image for each Cys112 is similar to that of a valine residue (Fig. 6(c)). Like the Arg40···Asp99 salt bridges, the side-chains of Cys112$\beta1$ and Cys112$\beta2$ are very close to the molecular dyad at the $\beta1\beta2(\alpha1\beta1)$ interface. This results in steric conflict when both sulfhydryl groups are oriented toward the $\beta1\beta4(\alpha1\beta2)$ dyad. As a result, the two Cys112 residues must alternate conformations in unison, like the motion of a car's windshield wipers. The Cys112 packing defect is consistent with the increased reactivity of Cys112 relative to Cys93 and with the multiple Hg sites of a Cys112-mercuribenzoate adduct (Neer, 1970; Arnone & Briley, 1978).

Of the $CO\beta_4$ residues that adopt dual conformations and give rise to resolved, or partially resolved, electron density double images, only Arg40, Asp99 and Cys112 are located at subunit interfaces. Many other $CO\beta_4$ residues with dual conformations are surface residues that can be influenced by lattice contacts and where barriers to reorientation are the lowest (Table 1: and see Smith *et al.*, 1988). However, buried residues have also been modeled with dual conformations in several structures, and some $CO\beta_4$ residues with dual conformations are buried hydrophobic residues. It is interesting to note that while Phe71(E15) and Val98(FG5) exhibit similar disorder in all four subunits, Leu14(A11), Leu68(E12) and Leu75(E19) show visible signs of disorder in only one or two subunits (Table 1). The ability of Leu14$\beta3$ to adopt two conformations may be due to its contact with a disordered surface residue, Glu121(GH4)$\beta3$, but in the case of Leu68 and Leu75 it is not obvious why disorder is observed in only two subunits. However, since very small structural perturbations that correspond to a difference in free energy of only a few hundred calories

can significantly shift the equilibrium ratio of the two possible conformers for these residues, it is not surprising that it is difficult to understand the basis for side-chain disorder in every case. For example, a weak perturbation of say −400 cal/mol will shift the equilibrium between two conformers by exp(400 cal·mol^{-1}/RT), a factor of 2. Residues that have two conformations in approximately equal amounts are sensitive "energy indicators" because shifting the equilibrium constant from 1 to 2 would likely result in an obvious difference in the corresponding electron density image for the side-chain. On the other hand, if one conformer is favored by a factor of 100 or 200 only the dominate conformation would be observed.

(iv) *The $\beta1\beta4(\alpha1\beta2)$ interface is "double-jointed"*

The interdigitation patterns of the $\alpha1\beta2$ interface of the $\alpha_2\beta_2$ tetramer and the corresponding $\beta1\beta4$ interface of $CO\beta_4$ are shown schematically in Figure 7. In $\alpha_2\beta_2$ Hb, the switch region is defined by the interaction of the $\alpha1$ C helix and CD corner with the $\beta2$ FG corner and G helix, and the joint region is defined by the interaction of the $\beta2$ C helix with the $\alpha1$ FG corner and G helix (Baldwin & Chothia, 1979). Although the switch and joint regions are formed from homologous portions of α and β subunits that are related by a pseudo 2-fold axis of symmetry, in deoxyHb the switch and joint structures differ significantly in detail. His97(FG4)$\beta2$ is positioned between Pro(CD2)$\alpha1$ and Thr41(C6)$\alpha1$ in the deoxyHb switch region, while the corresponding joint residue Arg92(FG4)$\alpha1$ is situated between Arg40(C6)$\beta2$ and Trp37(C3)$\beta2$. After the transition to the R (or R2) state in liganded Hb, switch residue His97(FG4)$\beta2$ jumps over a turn of 3_{10} helix to interdigitate between Thr41(C6)$\alpha1$ and Thr38(C3)$\alpha1$. In the joint, only a small sliding motion occurs and residue Arg92(FG4)$\alpha1$ remains positioned between Arg40(C6)$\beta2$ and Trp37(C3)$\beta2$. That is, in liganded Hb the switch and joint regions have the same interdigitation pattern and the $\alpha1\beta2$ interface is much more symmetric than it is in the deoxyHb $\alpha1\beta2$ interface (Dickerson & Geis, 1983). The interdigitation pattern of the $\beta1\beta4(\alpha1\beta2)$ interface in $CO\beta_4$ mimics that of the R and R2 states of liganded $\alpha_2\beta_2$ Hb. In the region that corresponds to the switch, residue His97(FG4)$\beta4$ is positioned between Arg40(C6)$\beta1$ and Trp37(C3)$\beta1$, while in the region that corresponds to the joint, His97(FG4)$\beta1$ is positioned between Arg40(C6)$\beta4$ and Trp37(C3)$\beta4$ (see Fig. 7). The 222 symmetry of the $CO\beta_4$ homotetramer requires that the $\beta1\beta4(\alpha1\beta2)$ interface must consist of two switch-like regions, two joint-like regions, or two structurally identical regions that are not analogous to either the switch or joint. It is clear from the foregoing analysis that the $CO\beta_4$ tetramer is in fact "double-jointed". In the accompanying paper, it is shown that the $\beta1\beta4(\alpha1\beta2)$ interface is double-jointed in deoxyβ_4 as well, confirming previous predictions (Perutz & Mazzarella, 1963; Benesch & Benesch, 1974) that the β_4 tetramer does not undergo large ligand-induced changes in quaternary structure.

(v) *The relative stabilities of the β_4 and $\alpha_2\beta_2$ interfaces*

Extensive studies have been published on the thermodynamics of subunit assembly in Hb as well as the isolated α and β-chains. The $\alpha_2\beta_2$ tetramer assembles *via* a stable $\alpha\beta$ dimer intermediate:

$$2\alpha + 2\beta \rightleftharpoons 2\alpha\beta \rightleftharpoons \alpha_2\beta_2$$

where the free energy of dimer formation is −16·3 kcal, and the free energy of tetramer formation is −8·0 kcal (Mills *et al.*, 1976; Turner *et al.*, 1981). This subunit assembly pathway reflects the relative stabilities of the $\alpha_2\beta_2$ interfaces. The most extensive and stable interface, the $\alpha1\beta1$ interface, forms first at very low subunit concentrations. The subsequent association of $\alpha1\beta1$ dimers results in the formation of three other types of subunit interfaces; the $\alpha1\beta2$ interfaces, the $\alpha1\alpha2$ interface, and the $\beta1\beta2$ interface. The fact that the $\alpha1\beta1$ dimer is the dominant species at low subunit concentrations implies this interface is energetically more stable than all the other subunit interfaces combined.

The self-association of isolated β subunits can be modeled accurately by a monomer-tetramer equilibrium with relatively little dimer formation:

$$4\beta \rightleftharpoons \beta_4$$

where the free energy of tetramer formation is −22 kcal (Valdes & Ackers, 1977, 1978; Philo *et al.*, 1988). The absence of a large population of dimers indicates that in the case of the β_4 homotetramer

deoxy $\alpha_2\beta_2$ hemoglobin (T)	liganded $\alpha_2\beta_2$ hemoglobin (R & R2)	β_4 hemoglobin
switch:	**switch:**	
α1 CD2 Pro 44 ⇐ 97 His FG4 β2	α1 CD2 Pro 44	β1 CD2 Glu 43
α1 C6 Thr 41	α1 C6 Thr 41 ⇐ 97 His FG4 β2	β1 C6 Arg 40 ⇐ 97 His FG4 β4
α1 C3 Thr 38	α1 C3 Thr 38	β1 C3 Trp 37
joint:	**joint:**	
α1 FG4 Arg 92 ⇒ 37 Trp C3 β2	α1 FG4 Arg 92 ⇒ 37 Trp C3 β2	β1 FG4 His 97 ⇒ 37 Trp C3 β4
40 Arg C6 β2	40 Arg C6 β2	40 Arg C6 β4
43 Glu CD2 β2	43 Glu CD2 β2	43 Glu CD2 β4

Figure 7. A diagram comparing the interdigitation patterns of the switch and joint regions of the $\alpha1\beta2$ interface of deoxy (T state) and liganded (R and R2 states) $\alpha_2\beta_2$ hemoglobin with the corresponding regions of the $CO\beta_4$ $\beta1\beta4$ interface.

the formation of the $\beta1\beta2(\alpha1\beta1)$ dimer interface is approximately equivalent energetically to the formation of the interdimer interfaces. In terms of the $\alpha_2\beta_2$ assembly pathway, either the $\beta1\beta2$ interface of the β_4 tetramer is less stable than the corresponding $\alpha1\beta1$ interface of $\alpha_2\beta_2$, or the interdimer interfaces are energetically more stable in β_4 than in $\alpha_2\beta_2$ or a combination of both.

To compare the interfaces of $CO\beta_4$ and oxyHb(R) the close subunit contacts are listed in Tables 4, 5 and 6. Since the liganded $\alpha1\beta1$ dimer is stable at concentrations where the $CO\beta_4$ tetramer dissociates completely to monomers, the $\alpha1\beta1$ interface must be much more stable than the corresponding $\beta1\beta2$ interface of $CO\beta_4$. One reason for this difference in stability is that while the $CO\beta_4$ $\beta1\beta2$ interface

Table 4

Subunit-subunit contacts of the $\alpha1\beta1$ interface of oxyHb(R) and the corresponding $CO\beta_4$ interface

oxyHb(R)† $\beta1(\beta2)$ residue	$\alpha1(\alpha2)$ residue	Atoms		Distance (Å)‡		$CO\beta_4$ $\beta2(\beta4)$ residue	$\beta1(\beta3)$ residue	Atoms		Distance (Å)‡	
Arg(B12)30β	His(H5)122α	N^{η}	$N^{\delta1}$	2·75	H	Arg(B12)30β	Gln(H5)127β	N^{η}	$O^{\varepsilon1}$	2·78 (4)	H ⇐
Arg(B12)30β	Phe(GH5)117α	$N^{\eta1}$	O	3·08	H	Arg(B12)30β	Phe(GH5)122β	$N^{\eta1}$	O	2·81 (1)	H ⇐
Val(B15)33β	Pro(H2)119α	C^{γ}	O	3·37							
						Tyr(C1)35β	Gln(H9)131β	O^{η}	$N^{\varepsilon2}$	3·54 (6)	
Met(D6)55β	Pro(H2)119α	C^{ε}	C^{β}	3·34							
Asn(G10)108β	His(G10)103α	O	$N^{\varepsilon2}$	3·08	H						
						Ala(G17)115β	Cys(G14)112β	C^{β}	O	3·59 (22)	
Ala(G17)115β	Ala(G18)111α	O	C^{α}	3·48		Ala(G17)115β	His(G18)116β	O	C^{α}	3·50 (16)	⇐
His(G18)116β	Ala(G17)110α	C^{α}	O	3·47		His(G18)116β	Ala(G17)115β	C^{α}	O	3·40 (7)	⇐
His(G18)116β	Pro(GH2)114α	$N^{\varepsilon2}$	O	2·89	H	His(G18)116β	Gly(GH2)119β	$N^{\varepsilon2}$	O	2·73 (8)	H ⇐
						His(G18)116β	Lys(GH3)120β	$N^{\varepsilon2}$	N	3·70 (23)	
						His(G18)116β	Phe(GH5)122β	$N^{\varepsilon2}$	O	3·42 (22)	
Gly(GH2)119β	Ala(G18)111α	C^{α}	O	3·45		Gly(GH2)119β	His(G18)116β	O	$N^{\varepsilon2}$	3·12 (37)	H ⇐
Phe(GH5)122β	Arg(B12)31α	O	$N^{\eta1}$	2·70	H	Phe(GH5)122β	Arg(B12)30β	O	$N^{\eta1}$	2·75 (3)	H ⇐
Pro(H3)125β	Leu(B15)34α	N	$C^{\delta2}$	3·37							
Gln(H5)127β	Arg(B12)31α	$O^{\varepsilon1}$	N^{η}	2·78	H	Gln(H5)127β	Arg(B12)30β	$O^{\varepsilon1}$	N^{η}	2·79 (14)	H ⇐
Gln(H5)127β	Ser(B16)35α	C^{γ}	O^{γ}	3·44							
Ala(H6)128β	Ser(B16)35α	C^{α}	O^{γ}	3·49							
Gln(H9)131β	His(G10)103α	$O^{\varepsilon1}$	$C^{\varepsilon1}$	3·08	H						

† Calculated from Protein Databank entry 1HHO (Shaanan, 1983).

‡ All distances are given as an average value with the standard deviation of the mean × 100 in parentheses. Interfaces were defined using a 3·5 Å cutoff and at least one interaction is <3·5 Å in either $\beta1\beta2$ or $\beta3\beta4$ interfaces; H, hydrogen bond <3·2 Å; ⇐, interaction conserved between $\alpha_2\beta_2$ and β_4 hemoglobin.

Table 5

Subunit-subunit contacts of the $\alpha1\beta2$ interface of oxyHb(R) and the corresponding $CO\beta_4$ interface

oxyHb(R) $\beta2(\beta1)$ residue	$\alpha1(\alpha2)$ residue	Atoms†		Distance (Å)‡		$CO\beta_4$ $\beta4(\beta2)$ residue	$\beta1(\beta3)$ residue	Atoms†		Distance (Å)‡	
Pro(C2)36β	Arg(FG4)92α	O	C^{δ}	3·38							
						Trp(C3)37β	His(FG4)97β	C^{β}	O	3·41 (5)	
						Trp(C3)37β	Asp(G1)99β	$C^{\delta1}$	$C^{\delta2}$(1)	3·27 (3)	
Trp(C3)37β	Pro(G2)95α	$C^{\delta2}$	C^{δ}	3·42		Trp(C3)37β	Pro(G2)100β	$C^{\delta2}$	C^{δ}	3·56 (6)	⇐
Gln(C5)39β	Arg(FG4)92α	$O^{\varepsilon1}$	$N^{\eta1}$	3·18	H						
Arg(C6)40β	Thr(C6)41α	$N^{\eta1}$	O	3·41		Arg(C6)40β	Arg(C6)40β	C^{δ}(1)	N^{η}(2)	3·43 (3)	
						Arg(C6)40β	Phe(C7)41β	C^{ζ}(1)	C^{ζ}	3·19 (7)	
						Arg(C6)40β	Glu(CD2)43β	$N^{\eta1}$(2)	$O^{\varepsilon2}$(1)	2·89	SB △
						Arg(C6)40β	Leu(FG3)96β	N^{η}(2)	O	2·79 (1)	H
						Arg(C6)40β	His(FG4)97β	N^{ε}(1)	O	3·02 (14)	H
						Arg(C6)40β	Asp(G1)99β	$N^{\eta1}$(1)	$O^{\delta1}$(1)	2·70 (4)	SB
						Phe(C7)41β	Arg(C6)40β	C^{ζ}	C^{ζ}(2)	3·24 (6)	
						Leu(FG3)96β	Arg(C6)40β	O	N^{η}(1)	3·34 (67)	H
His(FG4)97β	Thr(C3)38α	O	$O^{\gamma1}$	3·22		His(FG4)97β	Trp(C3)37β	O	C^{β}	3·45 (12)	⇐
						His(FG4)97β	Arg(C6)40β	O	N^{ε}(2)	3·09 (1)	H
						Asp(G1)99β	Trp(C3)37β	$O^{\delta2}$(1)	$C^{\delta1}$	3·24 (6)	
Asp(G1)99β	Val(G3)96α	C^{γ}	C^{γ}	3·33							
						Asp(G1)99β	Asn(G4)102β	$O^{\delta2}$(1)	$N^{\delta2}$	2·73 (3)	H
Asn(G4)102β	Asp(G1)94α	$O^{\delta1}$§	$O^{\delta2}$	2·80	H	Asn(G4)102β	Asp(G1)99β	$N^{\delta2}$	$O^{\delta2}$(1)	2·76 (4)	H ⇐
						Tyr(HC2)145β	Trp(C3)37β	O^{η}	C^{β}	3·55 (7)	

† (1) Main conformer and (2) alternate conformer.

‡ As in Table 4 except: SB, salt bridge <3·2 Å; and △, interactions are asymmetric between $\beta1\beta4$ and $\beta2\beta3$ interfaces at Glu43β due to lattice contacts (this salt bridge probably does not exist in solution).

§ For a proper hydrogen-bonding pair, $\chi2$ in the atomic model needs to be rotated 180°.

Table 6

Subunit-subunit contacts of the αα interface of oxyHb(R) and the ββ interface of COβ4

oxyHb(R) α1 residue	α2 residue	Atoms†		Distance (Å)‡		$CO\beta_4$ β1(β2) residue	β3(β4) residue	Atoms†		Distance (Å)‡	
Val(NA1)1α	Ser(H21)138α	C^{γ}	O	3·07							
Val(NA1)1α	Arg(HC3)141α	N	O_T	2·24	SB	Val(NA1)1β	His(HC3)146β	C^{α}	O_T	3·26 (9)	
Leu(NA2)2α	Arg(HC3)141α	N	O_T	2·92	H	His(NA2)2β	His(HC3)146β	N	O_T	3·18 (19)	H ⇐
Lys(H10)127α	Tyr(HC2)140α	N^{ζ}	O	2·58	H	Lys(H10)132β	Tyr(HC2)145β	C^{ϵ}	O	3·73 (27)	
Lys(H10)127α	Arg(HC3)141α	N^{ζ}	O	2·40	SB	Lys(H10)132β	His(HC3)146β	C^{ϵ}	O	3·75 (26)	
Ser(H21)138α	Val(NA1)1α	O	C^{γ}	3·08							
Tyr(HC2)140α	Lys(H10)127α	O	N^{ζ}	2·58	H						
Arg(HC3)141α	Leu(NA2)2α	O_T	N	2·92	H	His(HC3)146β	His(NA2)2β	O_T	N	3·20 (2)	H ⇐
Arg(HC3)141α	Val(NA1)1α	O_T	N	2·24	SB	His(HC3)146β	Val(NA1)1β	O_T	C^{α}	3·17 (4)	
Arg(HC3)141α	Lys(H10)127α	O	N^{ζ}	2·40	SB						

† C-terminal oxygen denoted as O_T.
‡ As in Table 5.

retains many of the packing interactions that define the α1β1 interface (indicated by the ⇐ symbols in Table 4), the $CO\beta_4$ β1β2 interface is more loosely packed than its α1β1 counterpart. In particular, there are significant packing differences at the end of the B helix between these homologous interfaces. As seen in Figure 4(b), the B helix–H helix contact region is spread apart by ~1 Å in $CO\beta_4$ relative to oxyHb(R). This difference in packing is reflected in the number of β1β2(α1β1) close contacts (Table 4). Specifically, the $CO\beta_4$ β1β2 interface does not include close contacts between residues Pro125(H3) and Val33(B15), Gln127(H5) and Val34(B16) and Ala128(H6) and Val34(B16). In addition, the side-chain disorder and high level of reactivity of Cys112(G17) indicates that the center of the $CO\beta_4$ β1β2 interface is less tightly packed. Although it is difficult to assign free energies to these differences, they are probably the main reason for the reduced stability of the $CO\beta_4$ β1β2 interface relative to the α1β1 interface.

While the α1β2 interface and the analogous β1β4 interface of $CO\beta_4$ are both constructed mainly from the FG corners and C helices of the corresponding subunits, only three of the $\alpha_2\beta_2$ interactions are conserved in the β_4 tetramer (indicated by ⇐ symbols in Table 5) because of amino acid substitutions between α and β-chains. Due to these differences, the $CO\beta_4$ β1β4 interface is more tightly packed (Fig. 3(a)) and has twice as many close contacts (Table 5). Of particular interest is the Arg40(C6)···Asp99(G1) salt bridge, which is unique to the $CO\beta_4$ tetramer. This interaction, and the associated contacts that are created by burying the salt bridge in the center of the interface, result in a fourfold increase in the number of polar bonds at the $CO\beta_4$ β1β4 interface. Significantly, recent work by Baudin *et al.* (1993) indicates that several Arg40(C6) mutations destabilize the β_4 tetramer more than the $\alpha_2\beta_2$ tetramer. It seems reasonable to conclude that the $CO\beta_4$ β1β4 interface is more stable that its α1β2 counterpart in liganded Hb.

The α1α2 and β1β2 interfaces of liganded $\alpha_2\beta_2$ Hb are weak, poorly packed interfaces. In fact, the β1β2 interface does not include any contacts closer than 4 Å (Lesk *et al.*, 1985), and most of the close contacts in the α1α2 interface involve N and C-terminal residues with very high mobility. The $CO\beta_4$ symmetry-related β1β3 and β2β4 interface are also relatively weak (see Table 6), but they include anion binding sites that are not present in the liganded $\alpha_2\beta_2$ tetramer (Arnone *et al.*, 1982). This is consistent with the observation that high salt enhances tetramer formation in liganded β_4, but has the opposite effect on liganded $\alpha_2\beta_2$ Hb (Tainsky & Edelstein, 1973; Valdes & Ackers, 1977). The $CO\beta_4$ tetramer should be more stable than the $\alpha_2\beta_2$ tetramer, since the salt-enhanced β2β4 and β1β3 interactions tie down both ends of the central cavity, while the $\alpha_2\beta_2$ tetramer is only weakly tethered at one end.

In summary, the main structural features of the $CO\beta_4$ tetramer indicate that the β1β2 interface is less stable than its α1β1 counterpart in liganded Hb, while the β1β4 interface is more stable than the corresponding α1β2 interface of liganded Hb. If this reversal in subunit interface stabilities is the dominate structural reason for the different pathways of $CO\beta_4$ and $\alpha_2\beta_2$ assembly, then mutations that strengthen the $CO\beta_4$ β1β2 interface, or weaken the $CO\beta_4$ β1β4 interface, should alter the monomer-tetramer assembly mechanism to one in which a significant amount of dimer is observed. The mutation in Hb Kempsey (β99 Asp→Asn), for example, is of this type because the key Arg40β1···Asp99β4 interaction should be lost or significantly weakened, greatly destabilizing the $CO\beta_4$ β1β4 interface. Recent experiments by Ackers and co-workers indicate that Hb Kempsey β subunits do in fact assemble to homotetramers by a pathway that is characterized by a high population of stable dimer intermediates (G. K. Ackers, personal communication).

We thank Gary Ackers and Mike Doyle for valuable discussions and for providing unpublished results. We are grateful to Madeline Shea, John Tainer and Elizabeth Getzoff for helpful suggestions and the use of facilities. This work was supported by research grants GM-40852 and HL-40453 from the National Institutes of Health.

G.E.O.B. was the recipient of a predoctoral fellowship (training grant T32-GM08365) from the National Institutes of Health.

The refined coordinates (entry code 1CBM) of the $CO\beta_4$ tetramer have been deposited in the Brookhaven Data Bank, Brookhaven National Laboratory, Upton, NY.

References

Arents, G. & Love, W. E. (1989). *Glycera dibranchiata* hemoglobin structure and refinement at 1·5 Å resolution. *J. Mol. Biol.* **210**, 149–161.

Arnone, A. & Briley, P. D. (1978). Location of the heme iron atoms and characterization of the quaternary structure of the carbonmonoxy-β_4 tetramer. In *Biochemical and Clinical Aspects of Hemoglobin Abnormalities* (W. S. Caughey, ed.). pp. 93–107, Academic Press, New York.

Arnone, A., Briley, P. D., Rogers, P. H. & Hendrickson, W. A. (1982). Structure-function relationships in carbonmonoxy β_4 hemoglobin. In *Hemoglobin and Oxygen Binding* (Ho, C., ed.), pp. 43–57, Elsevier North Holland, New York.

Baldwin, J. & Chothia, C. (1979). Haemoglobin: the structural changes related to ligand binding and its allosteric mechanism. *J. Mol. Biol.* **129**, 175–220.

Baudin, V., Pagnier, J., Kiger, L., Kister, J., Schaad, O., Bihoreau, M. T., Lacaze, N., Marden, M. C., Edelstein, S. J. & Poyart, C. (1993). Functional consequences of mutations at the allosteric interface in hetero- and homo-hemoglobin tetramers. *Protein Sci.* **2**, 1320–1330.

Benesch, R. & Benesch, R. E. (1974). Homos and heteros among the hemos. *Science*, **185**, 905–908.

Benesch, R., Benesch, R. E. & Enoki, Y. (1968). The interaction of hemoglobin and its subunits with 2,3-diphosphoglycerate. *Biochemistry*, **61**, 1102–1106.

Borgstahl, G. E. O. (1992). High resolution X-ray diffraction studies of hemoglobin: ligand-induced tertiary structure movements in "locked" quaternary structures. Ph.D. thesis, The University of Iowa, Iowa City, IA.

Borgstahl, G. E. O., Rogers, P. H. & Arnone, A. (1993). The 1·9 Å structure of deoxyβ_4 hemoglobin. Analysis of the partitioning of quaternary-associated and ligand-induced changes in tertiary structure. *J. Mol. Biol.* **236**, 831–843.

Cambillau, C. (1989). In *Silicon Graphics Geometry Partners Directory*, (Silicon Graphics, Mountain View, CA, ed.), p. 69, Silicon Graphics, Mountain View, CA.

Derewenda, Z., Dodson, G., Emsley, P., Harris, D., Nagai, K., Perutz, M. & Reynaud, J.-P. (1990). Stereochemistry of carbon monoxide binding to normal human adult and Cowtown haemoglobins. *J. Mol. Biol.* **211**, 515–519.

Dickerson, R. E. & Geis, I. (1983). *Hemoglobin*. Benjamin/Cummings Publishing Company, Inc., Menlo Park, CA.

Fermi, G., Perutz, M. F., Shaanan, B. & Fourme, R. (1984). The crystal structure of human deoxyhaemoglobin at 1·74 Å resolution. *J. Mol. Biol.* **175**, 159–174.

Hendrickson, W. A. (1985). Stereochemically restrained refinement of macromolecular structures. *Methods Enzymol.* **115**, 252–270.

Howard, A. J., Gilliland, G. L., Finzel, B. C., Poulos, T. L., Ohlendorf, D. H. & Salemme, F. R. (1987). The use of an imaging proportional counter in macromolecular crystallography. *J. Appl. Crystallogr.* **20**, 383–387.

Ippolito, J. A., Alexander, R. S. & Chistianson, D. W. (1990). Hydrogen bond stereochemistry in protein structure and function. *J. Mol. Biol.* **215**, 457–471.

Jones, T. A. (1985). Interactive computer graphics: FRODO. *Methods Enzymol.* **115**, 157–189.

Kavanaugh, J. S., Rogers, P. H. & Arnone, A. (1992). High resolution X-ray study of deoxy recombinant human hemoglobins synthesized from β-globins having mutated amino termini. *Biochemistry*, **31**, 8640–8647.

Kuriyan, J., Wilz, S., Karplus, M. & Petsko, G. A. (1986). X-ray structure and refinement of carbonmonoxy (FeII)-myoglobin at 1·5 Å resolution. *J. Mol. Biol.* **192**, 133–154.

Kurtz, A., Rollema, H. S. & Baurer, C. (1981). Heterotropic interactions in monomeric β^{SH} chains from human hemoglobin. *Arch. Biochem. Biophys.* **210**, 200–203.

Lesk, A. M., Janin, J., Wodak, S. & Chothia, C. (1985). Haemoglobin: the surface buried between the $\alpha 1\beta 1$ and $\alpha 2\beta 2$ dimers in the deoxy and oxy structures. *J. Mol. Biol.* **183**, 267–270.

McRee, D. E. (1992). A visual protein crystallographic software system for x11/xview. *J. Mol. Graph.* **10**, 44–47.

Mills, F. C., Johnson, M. L. & Ackers, G. K. (1976). Oxygenation-linked subunit interactions in human hemoglobin: experimental studies on the concentration dependence of oxygenation curves. *Biochemistry*, **15**, 5350–5362.

Neer, E. J. (1970). The reaction of the sulfhydryl groups of human hemoglobin β_4. *J. Biol. Chem.* **245**, 564–569.

Peng, S. M. & Ibers, J. A. (1976). Stereochemistry of carbonylmetalloporphyrins. The structure of (pyridine)(carbonyl)(5, 10, 15, 20-tetraphenylprophinato) iron(II). *J. Amer. Chem. Soc.* **98**, 8032–8036.

Perutz, M. F. & Mazzarella, L. (1963). A preliminary X-ray analysis of haemoglobin H. *Nature (London)*, **199**, 639.

Phillips, S. E. V. (1980). Structure and refinement of oxymyoglobin at 1·6 Å resolution. *J. Mol. Biol.* **142**, 531–554.

Philo, J. S., Lary, J. W. & Schuster, T. M. (1988). Quaternary interactions in hemoglobin β subunit tetramers. *J. Biol. Chem.* **263**, 682–689.

Shaanan, B. (1983). Structure of oxyhaemoglobin at 2·1 Å resolution. *J. Mol. Biol.* **171**, 31–59.

Sheriff, S. (1987). Addition of symmetry-related contact restraints to PROTIN and PROLSQ. *J. Appl. Crystallogr.* **20**, 53–55.

Sheriff, S. & Hendrickson, W. A. (1987). Description of overall anisotropy in diffraction from macromolecular crystals. *Acta Crystallogr. sect. A*, **43**, 118–121.

Silva, M. M., Rogers, P. H. & Arnone, A. (1992). A third quaternary structure of human hemoglobin a at 1·7 Å resolution. *J. Biol. Chem.* **267**, 17248–17256.

Smith, J. L., Hendrickson, W. A., Honzatko, R. B. & Sheriff, S. (1986). Structural heterogeneity in protein crystals. *Biochemistry*, **25**, 5018–5027.

Smith, J. L., Corfield, P. W. R., Hendrickson, W. A. & Low, B. W. (1988). Refinement at 1·4 Å resolution of a model of erabutoxinb: treatment of ordered solvent and discrete disorder. *Acta Crystallogr. sect. A*, **44**, 357–368.

Svensson, L. A., Sjolin, L., Gilliland, G. L., Finzel, B. C. & Wlodawer, A. (1986). Multiple conformations of amino acid residues in ribonuclease A. *Proteins: Struct. Funct. Genet.* **1**, 370–375.

Tainsky, M. & Edelstein, S. J. (1973). Enhanced quaternary stability of β_4 hemoglobin in 2M sodium chloride. *J. Mol. Biol.* **75**, 735–739.

Tilton, R. F. & Petsko, G. A. (1988). A structure of sperm whale myoglobin at a nitrogen gas pressure of 145 atmospheres. *Biochemistry*, **27**, 6574–6582.

Turner, B. W., Pettigrew, D. W. & Ackers G. K. (1981). Measurement and analysis of ligand-linked subunit dissociation equilibria in human hemoglobins. *Methods Enzymol.* **76**, 596–628.

Tronrud, D. E., Ten Eyck, L. F. & Matthews, B. W. (1987). An efficient general-purpose least-squares refinement program for macromolecular structures. *Acta Crystallogr. sect. A*, **43**, 489–501.

Valdes, R. J. & Ackers, G. K. (1977). Thermodynamic studies on subunit assembly in human hemoglobin. *J. Biol. Chem.* **252**, 74–81.

Valdes, R. J. & Ackers, G. K. (1978). Self-association of hemoglobin β^{SH} chains is linked to oxygenation. *Proc. Nat. Acad. Sci., U.S.A.* **75**, 311–314.

Edited by P. E. Wright

(Received 2 September 1993; accepted 5 November 1993)